

## Article

# Shear-Wave Velocity Model from Site Amplification Using Microtremors on Jeju Island

Junkyoung Kim <sup>1</sup> , Dongkeuk Park <sup>2</sup>, Gitae Nam <sup>3,\*</sup> and Haiyoung Jung <sup>1,\*</sup> 

<sup>1</sup> Department of Fire and Disaster Prevention, Semyung University, 65 Semyung-ro, Jecheon-si 27136, Republic of Korea; kimjk3926@gmail.com

<sup>2</sup> Korean Radioactive Waste Society, 111 Daedeok-daero, 989 Beon-gil, Yuseong-gu, Daejeon 34057, Republic of Korea; k065pdk@daum.net

<sup>3</sup> Seoul Metropolitan Council, Urban Safety & Construction Committee, 15 Deoksugung-gil, Jung-gu, Seoul 04515, Republic of Korea

\* Correspondence: gogo7263@naver.com (G.N.); hyjung@semyung.ac.kr (H.J.)

**Abstract:** This study examines shear-wave velocity structures in the Jeju region utilizing horizontal-to-vertical spectral ratios (HVSRs) of environmental noise, focusing on identifying significant low-velocity layers (LVLs). Although conventional methodologies predominantly involve borehole and active seismic exploration, recent advancements in the diffuse-field theory of seismic waves have offered a theoretical foundation for this approach. In the volcanic region of Jeju Island characterized by unique geological features, a pervasive LVL composed of quaternary marine sediments and the Seoguipo sedimentary layer has been observed. These components are crucial for site amplification and attenuation in seismic microzonation. The present study introduces a novel discovery of a distinct LVL, specifically at the UDO site, suggesting that its origin may be attributable to a local magmatic intrusion event. Advanced algorithms and HVSР curve analysis have enabled reliable inversion processes, enhancing the comprehension of the subsurface geology of Jeju. These insights are essential for seismic microzonation practices and contribute significantly to the development of seismic design standards in the Jeju region.



**Citation:** Kim, J.; Park, D.; Nam, G.; Jung, H. Shear-Wave Velocity Model from Site Amplification Using Microtremors on Jeju Island. *Appl. Sci.* **2024**, *14*, 795. <https://doi.org/10.3390/app14020795>

Academic Editors: Rosa Nappi and Valeria Paoletti

Received: 14 December 2023

Revised: 10 January 2024

Accepted: 16 January 2024

Published: 17 January 2024



**Copyright:** © 2024 by the authors. Licensee MDPI, Basel, Switzerland. This article is an open access article distributed under the terms and conditions of the Creative Commons Attribution (CC BY) license (<https://creativecommons.org/licenses/by/4.0/>).

## 1. Introduction

The thickness of the sedimentary cover overlaying the earth's surface and the local shear-wave velocity structure, extending to depths of approximately 2–3 km, are critical parameters in both geotechnical engineering and geosciences. These parameters are influential in controlling site amplification and site attenuation (kappa) of ground motion during seismic events. The horizontal-to-vertical spectral ratios (HVSRs) of environmental noise have demonstrated effectiveness in investigating shear velocity profile layers across diverse geological contexts [1]. In this investigation, the local shear-wave velocity structures of the Jeju region were examined using HVSRs of environmental noise, aiming to identify the presence of a significant low-velocity layer (LVL) or a consortium of LVLs. Historically, conventional approaches for describing the mechanical properties of the ground for seismic microzonation have relied upon borehole drilling and active seismic prospecting. Over the past two decades, substantial advancements have been achieved in mapping the mechanical properties of both shallow subsoil and bedrock for local seismic microzonation, utilizing environmental noise recordings. This methodology involves employing a single station to estimate the HVSР curves. Numerous studies employing HVSР curves for site amplification characterization have utilized data sourced from background noise [2–5], coda wave seismic energy [6–10], and S-wave energy [11,12], thus allowing for amplification and attenuation in seismic microzonation in the volcanic region [13].

Specifically, the long-period HVSR of environmental noise has been effectively applied to ascertain the shear-wave velocity ( $V_s$ ) of deep sedimentary layers in various global locations, including the Kanto Plain in Japan [14], the Santa Clara Valley in California [15], and the Rhine Embayment in Germany [16]. Additionally, array configurations have been employed in certain studies [17] to estimate surface wave dispersion curves. Until recently, the HVSR curves of environmental noise were interpreted semi-empirically, viewed as either representing Rayleigh wave ellipticity or the amplitude ratio of the sum of Rayleigh and Love waves [18,19]. The advancements in diffuse-field theory [20,21] have led to the proposition that a theoretical formulation, instead of an empirical one, should be applied to multilayer stratum models with depth-dependent shear velocity. Research applying diffuse-field theory in this domain is being actively conducted by Kawase et al. [22], Kawase et al. [23], Lontsi et al. [24], and others, focusing on horizontally homogeneous multilayer models. Passive seismic techniques based on the measurements of environmental noise have proven effective in scenarios where alternative methods are impractical owing to either elevated environmental seismic noise or constrained budgets. These techniques offer substantial lateral coverage at manageable costs, rendering them particularly advantageous for seismic microzonation in regions of low seismicity and in developing countries. The present study aimed to analyze the shear velocity profile of a multilayer structure by applying diffuse-field theory.

Jeju Island, situated on the continental shelf south of the Korean Peninsula, measures approximately 70 km (EW) by 30 km (NS). As a volcanic island, it exhibits the geochemical characteristics of oceanic island basalt, originating from Pleistocene eruptions. Geologically, the Jeju region is markedly distinct from the inland areas of the Korean Peninsula, comprising the Halla volcanic edifice in its central region, a lava plateau in the east, and numerous cinder cones dispersed across the island [25]. Previous geophysical studies have established the existence of an LVL beneath the extrusive volcanic outcrops of Jeju Island. This LVL, varying in thickness from approximately 100 to 300 m and occurring at different depths, is believed to comprise quaternary marine sediments. Quite possibly, this LVL plays a crucial role in controlling both the site amplitude and site attenuation of ground motion for seismic microzonation in the Jeju region [26–32]. The vicinity of Jeju Island is characterized by relatively low seismic activity compared to other regions in Korea. Nevertheless, seismic design remains imperative for significant national infrastructures and utilities within the Jeju region, including the construction of new airports and potential nuclear power plants. The objective of this study is to furnish more dependable characteristics of seismic microzonation for Jeju Island by describing the significant LVLs or clusters of LVLs, employing the HVSR of environmental noises and their regional distribution.

For the analysis of HVSR curves, we utilized a substantial quantity of environmental noise data preceding the first P-phase arrival, which were recorded by the Korean National Seismic Network in the Jeju region, originating from the 9 Pohang earthquake series and the 15 Kumamoto earthquake series (main event: ML 7.3, JMA intensity 7). These datasets were selected owing to their comprehensive coverage of the Jeju area and the magnitude of the earthquakes, which ensured their detectability at most seismic stations in the region. The present findings are compared with those reported by preceding studies employing diverse geophysical methods, including borehole analysis [26], gravity and magnetic surveys [27], gravity studies [28], paleomagnetic research [29], seismic investigations [30], magneto-telluric (MT) assessments [31], and deep resistivity soundings [32], to ascertain the LVL of the Jeju region. We anticipate that our results will align with those of previous studies and potentially reveal new systematic LVLs that have not been documented previously. Furthermore, a novel hypothesis has been proposed regarding the origin of the LVL at the UDO site [26–32]. This research significantly advances the geological examination of the distinct geological units in the Jeju region, including the sea-origin U-formation and Seoguipo strata, with a focus on stratigraphic information directly or indirectly pertinent to the LVL. Additionally, it contributes to the field of seismic design engineering by facilitating the analysis of seismic hazards associated with seismic microzonation. This is achieved

through the examination of notable site amplification and attenuation phenomena in the Jeju region.

## 2. Ambient Noise Data

For the analysis of HVSR curves, we utilized a substantial amount of ambient noise recorded by the Korean National Seismic Network stations in the Jeju region during the Pohang and Kumamoto earthquakes. Specifically, the present evaluation involved 351 horizontal and vertical ambient noise recordings from 15 Kumamoto earthquakes at six stations (270 noise motions) and 9 Pohang earthquakes at three stations (81 noise motions) (Tables 1 and 2).

**Table 1.** Dates and seismic stations at which earthquakes occurred.

No.	Event Date	Latitude	Longitude	ML	Stations	Remarks
1	14 April 2016 21:26:00	32.70	130.80	6.5	GOS, HALB, JJB, MRD, SGP, SSP	Kumamoto Event
2	14 April 2016 22:07:00	32.80	130.80	5.7	GOS, HALB, JJB, MRD, SGP, SSP	Kumamoto Event
3	14 April 2016 22:38:00	32.70	130.70	5.0	GOS, HALB, JJB, MRD, SGP, SSP	Kumamoto Event
4	15 April 2016 00:03:00	32.70	130.80	6.4	GOS, HALB, JJB, MRD, SGP, SSP	Kumamoto Event
5	15 April 2016 01:53:00	32.70	130.80	4.8	GOS, HALB, JJB, MRD, SGP, SSP	Kumamoto Event
6	16 April 2016 01:25:00	32.80	130.80	7.3 (JMA Intensity 7)	GOS, HALB, JJB, MRD, SGP, SSP	Kumamoto Event
7	16 April 2016 01:45:00	32.90	130.90	6.0	GOS, HALB, JJB, MRD, SGP, SSP	Kumamoto Event
8	16 April 2016 03:03:00	33.00	131.10	5.8	GOS, HALB, JJB, MRD, SGP, SSP	Kumamoto Event
9	16 April 2016 03:55:00	33.00	131.20	5.8	GOS, HALB, JJB, MRD, SGP, SSP	Kumamoto Event
10	16 April 2016 07:23:00	32.80	130.80	4.8	GOS, HALB, JJB, MRD, SGP, SSP	Kumamoto Event
11	16 April 2016 09:48:00	32.90	130.80	5.4	GOS, HALB, JJB, MRD, SGP, SSP	Kumamoto Event
12	16 April 2016 16:01:00	32.80	130.80	5.3	GOS, HALB, JJB, MRD, SGP, SSP	Kumamoto Event
13	17 April 2016 00:14:00	33.00	131.10	4.9	GOS, HALB, JJB, MRD, SGP, SSP	Kumamoto Event
14	19 April 2016 17:52:00	32.60	130.70	5.5	GOS, HALB, JJB, MRD, SGP, SSP	Kumamoto Event
15	19 April 2016 20:47:00	32.60	130.70	5.0	GOS, HALB, JJB, MRD, SGP, SSP	Kumamoto Event
16	15 November 2017 14:29:31	36.11	129.37	5.4	CJD, JJU, UDO	Pohang Event
17	15 November 2017 14:32:59	36.10	129.36	3.6	CJD, JJU, UDO	Pohang Event
18	15 November 2017 15:09:49	36.09	129.34	3.5	CJD, JJU, UDO	Pohang Event
19	15 November 2017 16:49:30	36.12	129.36	4.3	CJD, JJU, UDO	Pohang Event
20	19 November 2017 23:45:47	36.12	129.36	3.5	CJD, JJU, UDO	Pohang Event
21	20 November 2017 06:05:15	36.14	129.36	3.6	CJD, JJU, UDO	Pohang Event

**Table 1.** Cont.

No.	Event Date	Latitude	Longitude	ML	Stations	Remarks
22	25 December 2017 16:19:22	36.11	129.36	3.5	CJD, JJU, UDO	Pohang Event
23	11 February 2018 05:03:03	36.08	129.33	4.6	CJD, JJU, UDO	Pohang Event
24	10 February 2019 12:53:38	36.16	129.90	4.1	CJD, JJU, UDO	Pohang Event

**Table 2.** Seismic stations and their distances from the main event epicenter.

No.	Station	Latitude	Longitude	Sensor	Distance [km]
1	GOS	33.3003	126.2100	ES-T	431.65
2	HALB	33.4019	126.2729	ES-DH	427.20
3	JJU	33.4294	126.5463	ES-T	394.14
4	SGP	33.2587	126.4983	ES-T	411.63
5	SSP	33.3873	126.8801	ES-T	371.16
6	CJD	33.9594	126.2934	ES-T	368.24
7	UDO	33.5228	126.954	ES-T	362.50
8	MRD	33.1166	126.2659	ES-T	424.94
9	JJB	33.4515	126.6559	ES-DH	392.85

Table 1 outlines the date and time of occurrence, the geographic coordinates of the 15 Kumamoto and 9 Pohang earthquake epicenters, and the station names where ground motions were recorded. We processed 351 ambient noise recordings (comprising two horizontal and one vertical component) with 5% cosine tapering. Corrections were enacted to the DC components and linear trends prior to calculating the HVSR for each station, aiming to eliminate traffic and other cultural noises contingent on the data. These data comprised ambient acceleration records.

In 2016, Kyushu Island in southwest Japan experienced a sequence of 15 earthquakes in the Kumamoto region. The mainshock, registering a magnitude of 7.3, was detected by seismic stations in the Jeju area, located approximately 367–429 km from the epicenter. The earthquakes had a focal depth of 10–20 km, indicative of mid-crustal seismic activity. These seismic events resulted in over 48 fatalities and caused substantial damage to buildings and structures in both the Jeju area and inland cities.

Given that ambient noise from the Kumamoto earthquake series was not captured at the JJU and SGP stations nor at the newly installed UDO station, the HVSR data were analyzed using ambient noise from the 2017 Pohang earthquake series (depicted in Figure 1 and Table 1) with magnitudes ranging from 3.5 to 5.4, subsequent to the Kumamoto earthquake series. This methodology is advantageous because it eliminates the need for extensive and expensive recording activities to acquire environmental noise data at each site, thereby resulting in substantial financial savings.

Nevertheless, there are challenges associated with acquiring data at precise locations and times. However, this limitation can be mitigated if the National Seismic Network provides comprehensive coverage of the entire Jeju area. The duration of the noise motion recordings was set to be 600 s or more, depending on the specific data, with a ground motion acceleration sampling interval of 0.01 s. In particular, two types of digital sensors, ES-DH and ES-T, were employed. Each seismic station recorded three-component measurements using a permanent acquisition system.

The HVSR was calculated by performing the fast Fourier transform on one vertical and two horizontal components of the noise recordings. This involved utilizing time windows of 20–30 s, tapered with a 5% cosine function prior to the spectrogram computation for each noise component. The HVSR curves were then smoothed using the Konno and Ohmachi et al. [33] window, applying a b value of 40. Spectral ordinates relative to the horizontal

components were geometrically averaged and divided by the vertical spectral ordinate to calculate the HVSR function, employing the GEOPSY software ver. 2.1 [34]. The final HVSR was derived by averaging the results obtained from considering 20–25-time windows with a certain overlap between them.

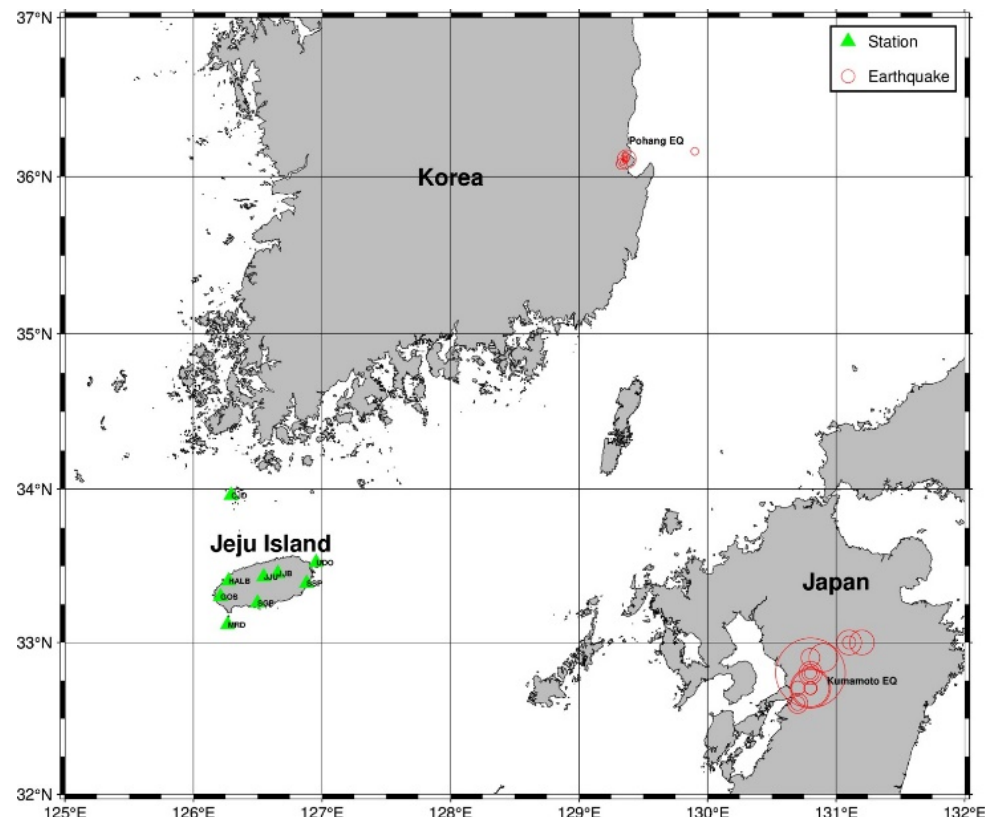


**Figure 1.** Locations of Pohang earthquake series, Kumamoto earthquake series (red circles), and nine seismic sites (green triangles).

### 3. Methods

The inversion of HVSR curves for Vs profiles presents a costly endeavor, primarily due to the extensive and labor-intensive search required in the parameter space. This complexity is further compounded by the prolonged convergence times or the potential failure to converge, a consequence of the highly ill-posed nature of the nonlinear inversion problem, such as determining the Vs structure [35,36].

To overcome this challenge and improve the reliability of the results, a key strategy adopted in this study involved the independent use of two inversion algorithms for the same observed HVSR curve. Thus, an HVSR inversion scheme was executed using Monte Carlo (MC) simulations and simulated annealing (SA) algorithms. These algorithms are renowned for their effectiveness in computing nonlinear inversion processes [37–41].

An additional strategy involved permitting a broad spectrum of variances in the observed HVSR curves during the inversion process. To address the ill-posed inversion condition, the inversion scheme was applied across a range of HVSR curve variances (0.25, 0.5, 0.75, 1.0, 1.25, 1.5, 1.75, 2.0, 2.25, and 2.5). This approach facilitated independent observation of the HVSR for each algorithm, followed by a comprehensive evaluation.

As a third strategy, to refine the initial parameter space exploration and intensify the search for viable solutions, initial boundary limits for the parameters were established based on previous studies conducted in the study area. Incorporating insights from all prior studies, initial values for Vs, layer thickness, and density were assigned for the inversion process. The initial ranges of the inversion parameters for the sites under investigation are enumerated in Table 3 [26–32].

**Table 3.** Range of initial inversion parameters for inversion.

Layer	Thickness (m)	Vs (m/s)	Density (kg/cm <sup>3</sup> )
1	50–150	1600–1800	1600–1800
2	50–150	1800–2000	1600–1900
3	50–250	1800–2500	1800–2100
4	50–250	1800–2500	1900–2200
5	50–250	1800–2500	1900–2200
6	50–250	2000–3000	2000–2200
7	Basement	2000–3000	2000–2200

To address the complexities inherent in a highly ill-posed nonlinear inversion process, two critical steps were implemented to establish the initial shear-wave velocity profile for the inversion. The first step involved determining the initial values of the free parameters for an efficient nonlinear inversion, constrained within the predetermined search limits of the layer parameters, using a random search method. Based on these initial values, the second step entailed searching the parameter spaces for global minimum misfit. Previous sensitivity analyses have highlighted that the HVSR curve is predominantly influenced by the S-wave velocity, Vs, and the layer thickness [19,42].

The shear velocity profile in the Jeju region was examined by evaluating the misfit between the observed and synthetic HVSR curves, including an assessment of their shape characteristics such as the peak amplitude, number of peaks, and specific frequency. The misfit value is quantified as follows:

$$\Delta_{HV} = \sum_{i=1}^n \frac{(HV_{obs}(f_i) - HV_{th}(f_i))^2}{(HV_{obs}(f_i))^2}, \quad (1)$$

where  $\Delta_{HV}$  denotes the misfit value,  $HV_{obs}(f_i)$  indicates the HVSR of the observed environmental noise, and  $HV_{th}(f_i)$  represents the synthetic noise.

The synthetic HVSR curves were generated from the simulated values utilizing the principles of diffuse-field theory. The foundational work of Sanchez-Sesma et al. [37], which models microtremor HVSR for surface receivers, was adapted to the synthetic HVSR in this study. Under the basic assumption, the medium is conceptualized as a series of horizontal uniform layers overlying a homogeneous infinite half-space, the latter representing a rigid basement.

Parolai et al. [43] demonstrated that configuring the shear velocity profile with approximately eight layers yields reliable results for specific types of velocity structures, notably those with a cover layer thickness of several hundred meters, although this is contingent upon the varied conditions of the site. Inspired by previous research [26–32] and the insights of Parolai et al. [43], a seven-layer model was selected as the initial model. This decision was informed by examining the tendency of misfit value sizes after numerous inversion trials with five-, six-, seven-, and eight-layer velocity models, along with local geological data. The six- and eight-layer velocity models often resulted in outcomes that were physically inconsistent with the existing geological and geophysical studies. Therefore, in this study, inversions were conducted on a Vs profile comprising seven layers, including the basement, as the initial model. Table 4 presents the initial seven-layer model for the Jeju region, established prior to the aforementioned random search stage.

For each inversion algorithm, an initial population of 100 individuals was utilized to randomly search for Vs and layer thickness, based on a given input HVSR curve. To ascertain the global optimal solution, iterations were terminated when no further notable reduction in the misfit was observed for each inversion algorithm. At each site, greater emphasis was placed on the modal value of the most frequently mapped velocity models, indicated by darker colors, rather than on the less frequently mapped sections of layers, to determine the optimal velocity model. In cases where the modal value was not distinctly

observable, the optimal velocity model was determined based on the average value of the corresponding section.

**Table 4.** Resonance frequency and maximum resonance amplitudes at the 9 sites.

Site Name	Resonance Frequency (Hz)	Maximum Amplitude at Resonance Frequency
CJD	N/A	N/A
GOS	0.36 and 1.46	4.33 and 3.39
HALB	0.37	3.70
JJB	0.35	4.34
JJU	0.42	3.88
MRD	0.43	3.36
SGP	0.42	3.88
SSP	0.43	4.99
UDO	0.33	3.20

The inversion process was conducted employing 10 variance bounds to examine the HVSR for each algorithm. In this study, where the MC and SA algorithms were used, typically 20 inversion outcomes were generated per session. If the velocity model failed to converge satisfactorily after a single inversion session, the process utilizing the two algorithms was repeated one or two additional times. This repetition was carried out until the modal models were sufficiently delineated, evident by their darker mapping, utilizing the results of from 40 to 60 inversions. Moreover, the reflection coefficients (RCs) of the Vs profile were calculated using the elastic impedance, defined as the product of Vs (in m/s) and density (in kg/cm<sup>3</sup>). This metric signifies the degree of contrast in the velocity and density between adjacent layers. The magnitude and corresponding depth of the RC values derived from the inversion were also considered to ascertain an optimal velocity model. RC serves as a crucial indicator of discontinuity and contrast within a medium, based on the elastic impedance of the medium.

Given that seven layers were set as the initial values for the inversion process in this study, only the relatively large values among the six potential RC values were considered for the Vs profile. Consequently, the final velocity model was determined by comprehensively considering not only the modal models that were most frequently mapped, as indicated by a relatively darker color, but also the RC values.

#### 4. Results

Considering the search ranges of the parameter spaces reported in prior studies, a random search algorithm was employed during the initial phase of the nonlinear inversion process. This approach aimed to restrict the subvolume of the parameter space within the limits of the initial parameters. Subsequently, in the second phase, two nonlinear algorithms (MC simulations and SA), featuring broad variance ranges, were applied using the Vs model deduced in the initial step. The inversion was directed toward the optimal Vs structure model, and the results obtained from both algorithms were thoroughly evaluated for all sites, as elaborated below.

##### 4.1. CJD Station

Figure 2 presents the observed and inverted HVSR curves for the CJD site, situated in one of the seismotectonic provinces of the main Korean Peninsula and located on a small island near the southwestern part of the peninsula (refer to Figure 1). The observed curve is depicted by the red line, and the black dotted line represents the synthetic curve for the optimal velocity model derived from the inversion results. The alignment between the observed and inverted results was notably close. Although there was a minor discrepancy in the low-frequency band, this difference was minimal, particularly when

considering the expanded y-scale and compared to the other sites examined in this study, as discussed subsequently.

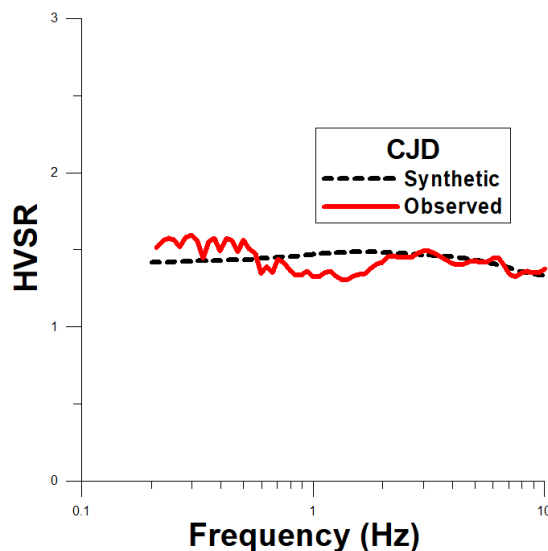


**Figure 2.** Observed and synthetic HVSRs of CJD site; the red line indicates the observed curve, and the black dotted line indicates the synthetic curve.

Both the MC and SA algorithms were utilized to invert the HVSR curves with a wide range of variance bounds (0.25–2.5) against the observed HVSR curves. Utilizing an initial seven-layer model, the MC algorithm revealed a misfit ranging from 3.84 to 22.79 across the entire frequency spectrum (0.1 Hz to 15 Hz), with the misfit value increasing drastically as the variance bound diminished. Similarly, the SA algorithm exhibited misfit values that escalated from 3.49 to 71.88 as the variance bound was reduced from 2.5 to 0.25, with the minimal misfit occurring at a variance bound of 2.5. Despite differences in the inversion algorithms and the extensive range of variances, the inversion results were similar in both the shape and amplitude of the HVSR curves, affirming the stability and reliability of the derived global optimal parameters.

In certain instances, HVSR curves may exhibit no pronounced peaks or may display amplitudes smaller than those observed at other sites across the entire frequency range, as exemplified by the CJD site. Owing to the inherent complexities of HVSR characteristics, which complicate the accurate estimation of Vs profiles due to uncertainties in the inversion process, sites with such profiles are often excluded from the inversion analysis. Despite its tectonic and geographic distinction from the Jeju region (as illustrated in Figure 1), the CJD site was incorporated into this study to facilitate a comparative analysis of the Vs structural characteristics between two tectonically divergent regions, i.e., Jeju Island and the inland areas.

As depicted in Figure 3, when applying two site classification codes (the national building code for site classification), the outcrops at the CJD sites, with velocities ranging from 1900 to 2000 m/s, were categorized as S<sub>A</sub> (the highest-quality outcrops) (refer to Table 5). This classification signifies that the near-surface sedimentary layer is not well-developed at this site [44].

In Figure 3, the layer profiles do not exhibit a starkly distinct velocity gradient; instead, there is a gradual increase in Vs with a subtle gradient. This pattern suggests a predominantly intact basement stratum structure extending to a depth of approximately 580–610 m. For site CJD, this weak velocity gradient might have contributed to the reduced amplitude of the HVSR across the entire frequency spectrum.

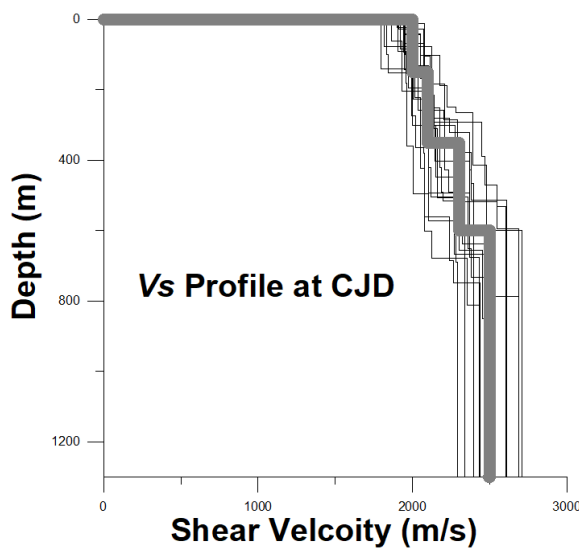


**Figure 3.** Estimated shear-wave velocity ( $V_s$ ) profile from the inversion of CJD site; the thin lines indicate all the inversion results, and thick gray line indicates the optimal  $V_s$  profile.

**Table 5.** Site classification standards (NOLIT, 20 2006).

Site Classification	Shear-Wave Velocity
$S_A$	>1500
$S_B$	760–1500
$S_C$	360–760
$S_D$	360–760
$S_E$	<180

Furthermore, the average RC of the  $V_s$  profile (as detailed in Table 6) demonstrated ranges between 0.002 and 0.05 across the seven strata, significantly lower than one-tenth of the RCs of the sites discussed later. Among these, three RC values exceeding 0.02 in Table 3 were selected and interpreted as indicative of four layers, inclusive of the basement. This interpretation—considering not only the relatively larger RC values amidst the minimal ones but also the frequently mapped inversion results—suggests that the site may be characterized by four layers including the basement. This finding implies a stable ground structure devoid of substantial disturbances.

**Table 6.** Depth, shear velocity ( $V_s$ ), and RC of CJD sites.

Layer	Lower Limit Depth of Each Stratum (m)	Shear Velocity (m/s)	RC		
			B (1–2)	B (2–3)	B (3–4)
1	140–160	1900–2100			
2	340–360	2000–2200	0.02		
3	590–610	2200–2400		0.05	
4	Bedrock	2400–2600			0.04

#### 4.2. GOS Site

Located on the western part of Jeju Island (Figure 1), the GOS site presented distinct characteristics in its HVSR curve analysis. Figure 4 illustrates both the observed and synthetic HVSR curves for the optimal  $V_s$  model at this site. The observed HVSR curve, represented by the red line, contrasts with the synthetic HVSR curve, indicated by the black dotted lines. These synthetic curves account for all inverted HVSR curves, excluding those deemed geologically implausible. The observed HVSR curve demonstrated two significant

peaks at frequencies of 0.36 Hz and 1.46 Hz, with corresponding peak amplitudes of 4.33 and 3.39, as noted in Table 4.

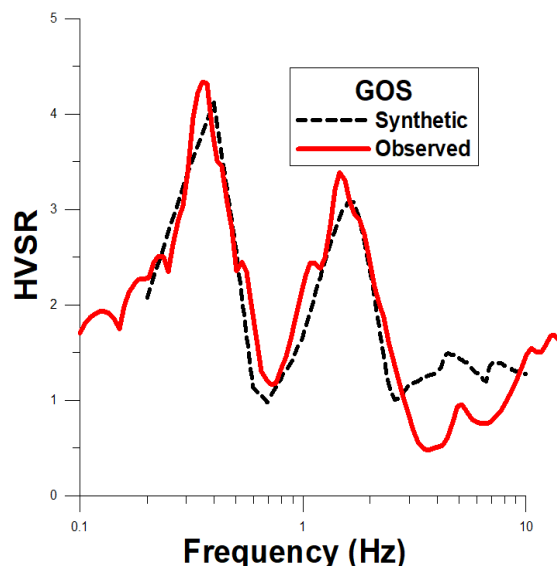


**Figure 4.** Observed and synthetic HVSRs of GOS site; the red line indicates the observed curve, and the black dotted line indicates the synthetic curve.

For the variance bounds ranging from 0.25 to 2.5, the misfit sizes obtained via inversion using the MC simulations were between 190.02 and 3.88, with the minimum misfit size observed at a variance of 2.5. The SA algorithm similarly revealed that the misfit sizes of the best-fit inversion model varied from 461.7091 to 4.292 over the same range of variance bounds. As observed at the CJD site, the misfit size decreased with increasing the variance bounds for both algorithms. Certain inverted-V models exhibited significant deviations from those used in previous studies, such as models with exceptionally thin layers (less than  $\sim 10$  m) or uniform Vs values that were either excessively high or low throughout the depth range. These models were subsequently excluded from further analysis. Despite variations in the inversion algorithms and the extensive range of permissible variances in the observed HVSR curves, the observed and synthetic HVSR curves for the optimal Vs model closely matched in amplitude and double peak frequencies, especially surrounding the first and second peaks.

A prior study addressing the topology of HV curves indicated that when HV curves exhibit two peaks, the lower-frequency peak typically corresponds to the fundamental frequency [45]. The second peak, characterized by a higher frequency and smaller amplitude, may be influenced by valley formations or the corresponding surface topology. However, the study posited that aside from the fundamental resonance peak, smaller peaks might lack geological relevance unless demonstrated by multiple other studies. Field investigations confirmed the absence of unusual topographical features such as valley development around the GOS site. Consequently, further inquiries into the cause of the double-peak phenomenon using alternative methodologies are warranted [40].

Figure 5 depicts the Vs profiles, showcasing both all the inverted and the optimal Vs models. In determining the optimal shear velocity profile, we focused on the darker segments, representing the more frequently mapped areas. The Vs map alternates between these frequently mapped dark regions and the less frequently mapped lighter areas. The modal-Vs model, characterized by darker sections and thus given more weight, was selected to ascertain the optimal model.

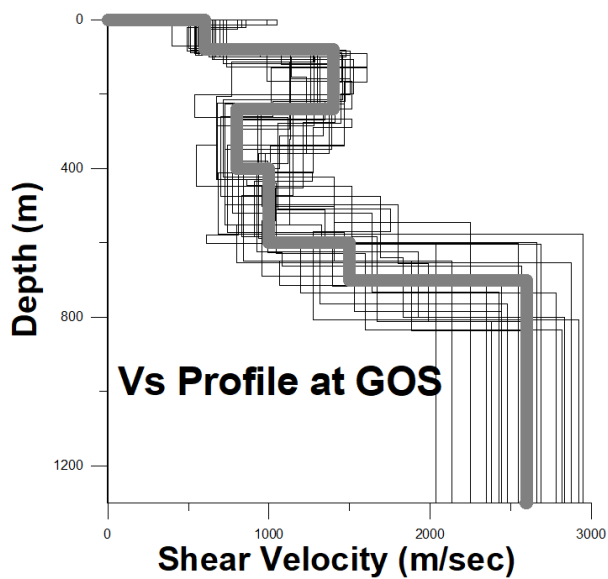


**Figure 5.** Estimated shear-wave velocity ( $V_s$ ) profile from the inversion of GOS site; the thin lines indicate all the inversion results, and thick gray line indicates the optimal  $V_s$  profile.

The  $V_s$  profile revealed a marked increase in velocity at depths of 70–90 m, with the velocities ranging from 500 to 700 m/s. This sharp velocity increase can be interpreted as a transition from surface sedimentary outcrops to a rock mass. Utilizing the site classification from the national building code based on the shear-wave velocity, as delineated in Table 5, the outcrops at the GOS sites with velocities of 500–700 m/s were classified as  $S_C$ . Beyond this, the velocity, ranging from 1300 to 1500 m/s, remained relatively constant up to depths of 230–250 m [44].

The third layer started at depths of 390–410 m, exhibiting significantly lower velocities (700–900 m/s) compared to the upper layers, indicative of the presence of the LVL. The identification of the LVL in the  $V_s$  profile represents one of the principal objectives of this study. Numerous previous studies have identified the LVL in Jeju, correlating it with marine-origin sediments of both the U-formation and the overlying Seoguipo sedimentary formation. Oh et al. [26] observed that marine sediments (U and Seoguipo formations) extensively overlay granitic basement rock across Jeju. Magnetotelluric (MT) studies [31], deep-resistivity soundings [32], and earlier MT surveys [27] have typically revealed a three-layered model: a resistive superstrate, a notably conductive substrate (with a thickness of approximately 100 m or more, varying by site), and a high-resistivity layer (basement). These conductive layers were consistently identified with marine-origin sediments, as confirmed by Oh et al. [26]. With increasing depth, there was a rapid doubling of the velocity observed at depths of approximately 590–610 m and 690–710 m. The latter depth range marks the onset of the deep basement.

In evaluating the frequency of the mapping models, along with the average RC values derived from the two different algorithms and the broad ranges of variances against the observed HVSR curve, several significant RC values were noted, as outlined in Table 7. These included four large positive peaks (0.43, 0.11, 0.20, and 0.27) and one large negative peak (−0.30). The first substantial positive RC, 0.40, was associated with the transition from the surface outcrop to the rock mass or surface bedrock, extending to a depth of 230–250 m. Note that larger RC values indicate a greater velocity differential across layer boundaries.

**Table 7.** Depth, shear velocity (Vs), and RC of GOS site.

Layer	Lower Limit Depth of Each Stratum (m)	Shear Velocity (m/s)	RC				
			B (1–2)	B (2–3)	B (3–4)	B (4–5)	B (5–6)
1	70–90	500–700	0.40				
2	230–250	1300–1500		(−) 0.27			
3	<b>390–410</b>	<b>700–900</b>			0.11		
4	590–610	900–1100				0.11	
5	690–710	1400–1600				0.20	
6	basement	2500–2700					0.27

At a depth of 230–250 m, the third layer begins, marked by a substantial negative RC of  $-0.30$ , indicative of the LVL. The Vs profile further revealed two additional velocity increments at depths of 390–410 m ( $RC = 0.11$ ) and 590–610 m ( $RC = 0.20$ ). Ultimately, as the depth extends and merges into the deep basement at approximately 690–710 m, an RC of 0.27 was observed. The depth, sign, and magnitude of these RC values aligned well with the transitions, velocity jumps, and the LVL identified in the site profile of the GOS. Therefore, the final velocity model for the GOS site was interpreted as comprising six layers, including the deep basement. This interpretation was based on a comprehensive assessment of not only the modal models that were frequently mapped, as denoted by their relatively darker color, but also the average RC values, as depicted in Figure 5. The Vs profile suggests the existence of several distinct layers, including the surface sedimentary layer, shallow rock masses, LVL, and the deep basement.

#### 4.3. HALB Site

The HALB site, situated on the western part of Jeju Island, exhibited characteristics similar to those of the GOS site (Figure 1). Figure 6 presents the observed and synthetic HVSR curves for the optimal Vs structure model at the HALB site. The observed HVSR curve demonstrated a significant peak at a frequency of 0.37 Hz, with a corresponding peak amplitude of 3.70, as noted in Table 4.

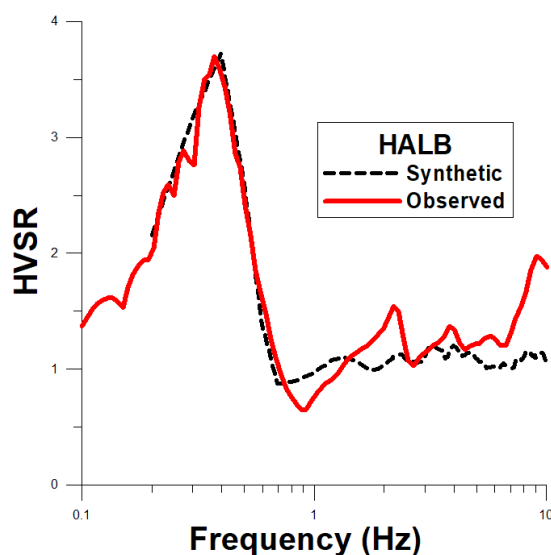


**Figure 6.** Observed and synthetic HVSRs of HALB site; the red line indicates the observed curve, and the black dotted line indicates the synthetic curve.

For the inversion process using the MC simulations and variance bounds ranging from 0.25 to 2.5, the misfit sizes were observed to vary from 156.1 to 0.13, with the smallest misfit occurring at a variance of 2.5. Similarly, the SA algorithm yielded misfit sizes for the best-fit inversion model ranging from 120.4 to 0.6 over the same variance bounds. Despite

the use of different inversion algorithms and the wide range of permissible variances, the observed and synthetic HVSR curves displayed a suitable alignment, especially around the peak part of the HVSR curves at frequencies of approximately 0.3 to 0.4 Hz (Table 4).

Figure 7 illustrates the Vs profiles at the HALB site, displaying all inverted and final optimal Vs models. In a manner similar to the previous site, the optimal model was determined by focusing on the more frequently mapped darker areas, or the modal model.

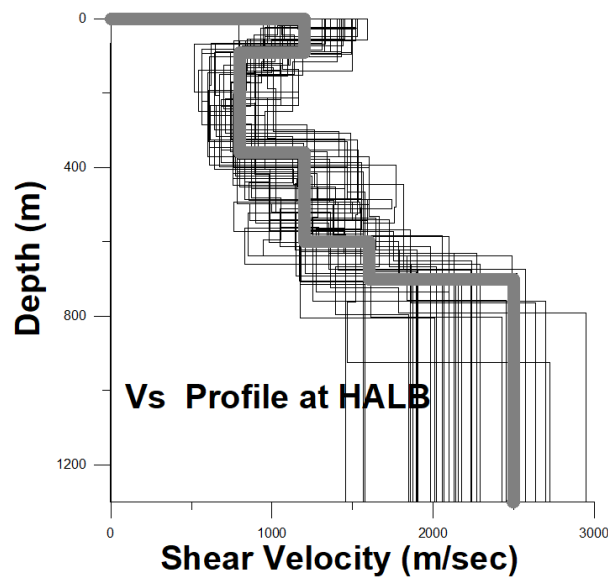


**Figure 7.** Estimated shear-wave velocity (Vs) profile from the inversion of HALB site; thin lines indicate all the inversion results, and thick gray line indicates the optimal Vs profile.

The Vs models at the HALB site indicate an abrupt reduction in velocity from 1100 to 1300 m/s to 700–900 m/s at depths of 80–100 m. This shift is interpretable as a transition from the surface rock mass to the LVL. Applying the site classification method based solely on the outcrop shear-wave velocity, as indicated in Table 5, the outcrops at the HALB sites (1100–1300 m/s) were categorized as S<sub>B</sub>. The LVL remained nearly consistent at depths of 350–370 m. As the depth increased to 590–610 m, a velocity increment was observed, followed by an encounter with the basement at depths of approximately 690–710 m [45].

The Vs profile in Figure 7 illustrates varying degrees of uncertainty across different depth ranges, with notably greater uncertainty observed in velocities below 690–710 m compared to other depth ranges. The discrepancies in the inverse algorithms did not yield significant differences in the basement velocity. Conversely, larger variances in the observed HVSR curve included reduced uncertainties in the inversion, especially in determining velocities below depths of 690–700 m. Consequently, to diminish the uncertainty of the Vs structure, future studies should consider various methodologies, such as augmenting the variance of the observed HVSR curve to a greater extent.

Table 8 includes the average RC values derived from all the inversion processes, providing additional insights into the Vs profiles. These average RC values revealed one large negative peak (−0.20) and three large positive peaks (0.20, 0.14, and 0.22). These peaks corresponded to significant contrasts in the Vs profile, including both decreases and increases in velocity. The first substantial negative RC peak of −0.20, at depths of 80–100 m, denotes the transition from the surface outcrop to the LVL, marked by a considerable velocity reduction of 400 m/s, extending to depths of 350–370 m. Beyond this depth, three velocity increments (0.20, 0.14, and 0.22) were encountered, culminating in the deep basement at depths of 690–710 m. The depth, sign, and magnitude of the RC aligned well with the transitions, velocity jumps, and LVL.

**Table 8.** Depth, shear velocity ( $V_s$ ), and RC of HALB site.

Layer	Lower Limit Depth of Each Stratum (m)	Shear Velocity (m/s)	RC			
			B (1–2)	B (2–3)	B (3–4)	B (4–5)
1	80–100	1100–1300	(–) 0.20			
2	<b>350–370</b>	<b>700–900</b>		0.20		
3	590–610	1100–1300			0.14	
4	690–710	1500–1700				0.22
5	Basement	2400–2600				

Therefore, the final velocity model for the HALB site was interpreted as comprising five layers. This interpretation was derived by holistically considering both the frequently mapped models, as indicated by their relatively darker color, and the average RC values, as depicted in Figure 7. Compared to the GOS site in the same western region, notable differences were observed in the upper boundary depth of the LVL at 230–250 m (GOS) versus 350–370 m (HALB), although the lower boundary depths were similar at 390–410 m (GOS) and 350–370 m (HALB). Additionally, the commencement depth of the basement was nearly identical at both sites.

#### 4.4. JJB Site

The JJB site is situated in the northern region of Jeju Island, as illustrated in Figure 1. Figure 8 displays the observed and synthetic HVSR curves for the optimal  $V_s$  model at this site. The observed HVSR curve demonstrated a notable peak at a frequency of 0.35 Hz, with a corresponding peak amplitude of 4.34, as detailed in Table 4. For the variance bounds ranging from 0.25 to 2.5, the misfit sizes from the MC simulations varied from 106.22 to 2.09. Similarly, the SA algorithm produced misfit sizes for the best-fit inversion model ranging from 168.60 to 1.45 over these variance bounds. Consistent with the observations at previous sites, the misfit size decreased with increasing the variance bounds for both algorithms. Despite the use of different inversion algorithms and the extensive range of permissible variances, the synthetic HVSR curve for the optimal  $V_s$  model closely aligned with the observed curve, particularly around the peak frequencies of approximately 0.3 to 0.4 Hz.

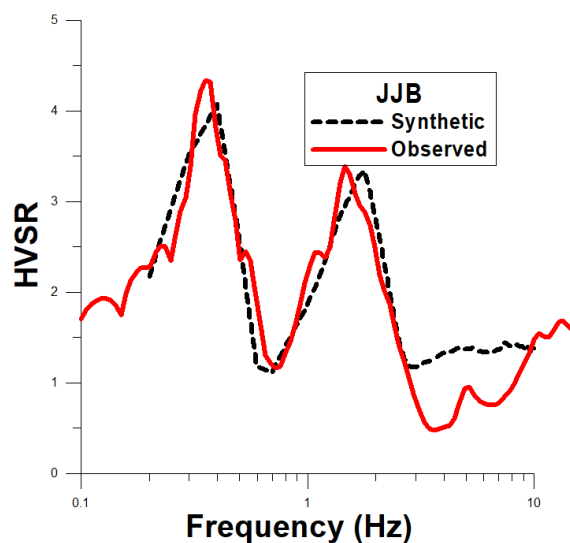


**Figure 8.** Observed and synthetic HVSRs of JJB site; the red line indicates the observed curve, and the black dotted line indicates the synthetic curve.

Figure 9 presents the  $V_s$  profiles at the JJB site, showcasing all inverted and optimal  $V_s$  models. In determining the optimal shear velocity profile, greater emphasis was placed on

the darker segments, which represent the more frequently mapped areas. Based on all the inversion results, excluding several geologically implausible values, the Vs profile up to a depth of 70–90 m showed the first layer with a velocity of 900–1100 m/s. Employing the site classification method based on surface shear-wave velocity, as indicated in Table 5, the outcrops at the JJB sites (600–700 m/s) were categorized as  $S_B$ . The second layer extended to depths of 240–260 m with a velocity of 1200–1400 m/s. The third layer, exhibiting a significant velocity reduction of approximately 600 m/s to 600–800 m/s, was identified as the LVL, extending from 240–260 m to 540–560 m in depth. With increasing depth, the fourth layer extended to 640–660 m, where the deep basement commences [45].

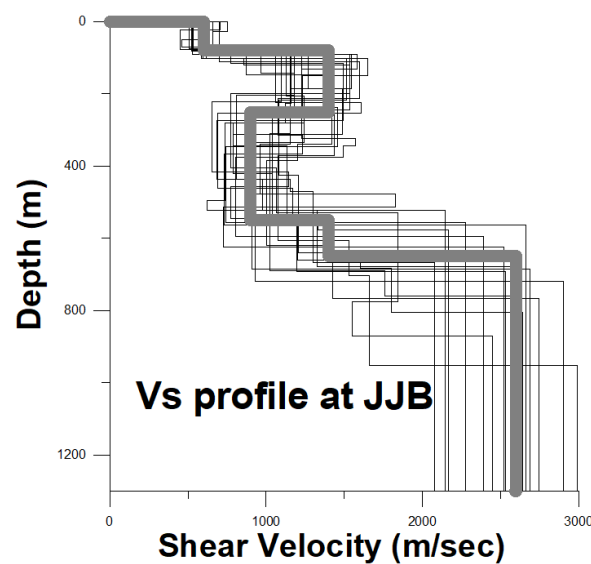


**Figure 9.** Estimated shear-wave velocity (Vs) profile from the inversion of JJB site; the thin lines indicate all the inversion results, and thick gray line indicates the optimal Vs profile.

The average RC values at the JJB site, as listed in Table 9, exhibited three large positive peaks (0.13, 0.22, and 0.37) and one large negative peak (−0.30). The first significant positive RC value of 0.13, occurring at a depth of 70–90 m, corresponded to the transition from the sedimentary outcrop to the surface basement. The second largest RC, −0.30, at a depth of 240–260 m, indicates a sudden decrease in velocity, marking the encounter with the LVL. With increasing depth, the average RC was 0.22 at 540–560 m and ultimately 0.37 at 640–660 m. Consequently, the final velocity model at the JJB site was interpreted as comprising five layers, including the basement, as illustrated in Figure 5. This interpretation was derived by considering both the frequently mapped models, indicated by their relatively darker color, and the average RC values. The depth, sign, and magnitude of the RC aligned well with the depth of transition, velocity jump, and LVL at the JJB site. Although the depth range and thickness of the low-velocity layer varied among sites, the presence of the LVL was similarly identified at the JJB site.

**Table 9.** Depth, shear velocity (Vs), and RC of the JJB site.

Layer	Lower Limit Depth of Each Stratum (m)	Shear Velocity (m/s)	B (1–2)	RC B (2–3)	B (3–4)	B (4–5)
1	70–90	900–1100				
2	240–260	1200–1400	0.13			
3	540–560	600–800		(−) 0.30		
4	640–660	1000–1200			0.22	
5	Basement	2300–2500				0.37

#### 4.5. JJU Site

The JJU site, also located in the northern region and similar to the JJB site, is depicted in Figure 1. Figure 10 presents the observed and synthetic HVSR curves for the optimal Vs model. The observed HVSR curve demonstrated a prominent peak at a frequency of 0.42 Hz, with a corresponding peak amplitude of 3.88, as noted in Table 4. For the variance bounds ranging from 0.25 to 2.5, the misfit sizes from the MC simulations varied from 342.74 to 3.33. The SA algorithm similarly produced misfit sizes for the best-fit inversion model ranging from 316.85 to 3.15 over the same variance bounds. As observed at the previous sites, the misfit size decreased with increasing variance bounds for both algorithms. Despite the differences in the inversion algorithms and the extensive range of permissible variances, the observed and synthetic HVSR curves showed a strong correlation, with the exception of certain frequency ranges (3–9 Hz).

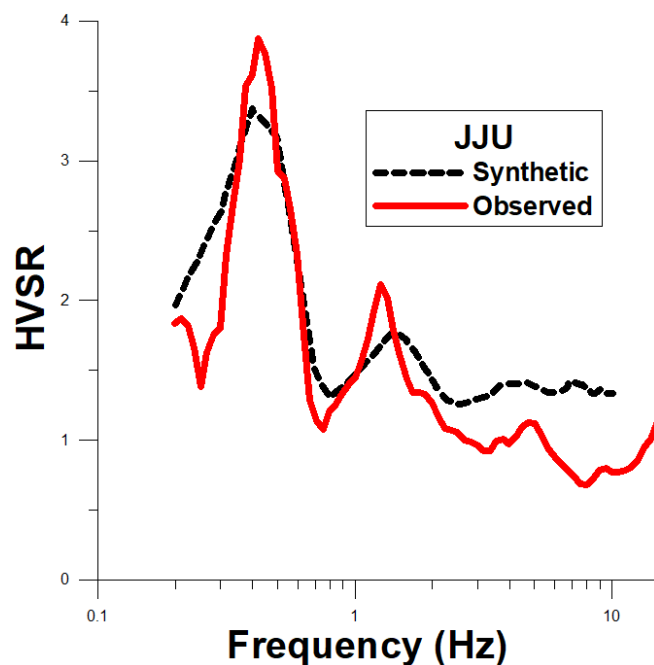


**Figure 10.** Observed and synthetic HVSRs of JJU site; the red line indicates the observed curve, and the black dotted line indicates the synthetic curve.

Figure 11 displays the Vs profiles at the JJU site, showcasing both the inverted and optimal Vs models. In determining the optimal shear velocity profile, greater emphasis was placed on the darker segments, which represent the more frequently mapped areas. The first layer formed a velocity range of 700–900 m/s up to a depth of 160–180 m. Utilizing the site classification method based on the surface shear-wave velocity, as indicated in Table 5, the outcrops at the JJU sites (700–900 m/s) were classified as  $S_B$ . The second layer, with velocities of 1300–1500 m/s, extended from 160–180 m to depths of 290–310 m. The third layer began with a slightly lower velocity of 900–1100 m/s, averaging a reduction of 400 m/s, and extended to depths of 490–510 m. This layer, exhibiting lower velocities, was consistent with the typical LVL identified across the Jeju region compared to the upper and lower strata. Finally, the velocity significantly increased to 2300–2500 m/s at depths of 690–710 m, indicative of the deep basement [45].

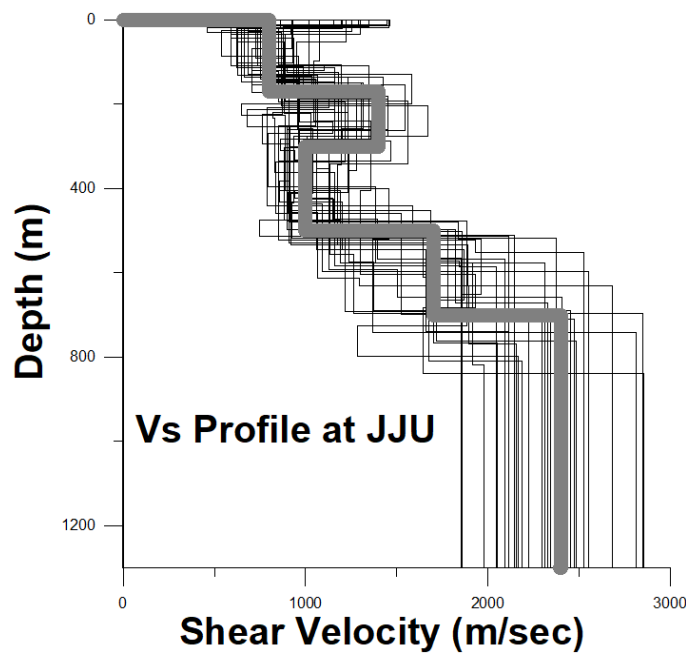


**Figure 11.** Estimated shear-wave velocity (Vs) profile from the inversion of JJU site; the thin lines indicate all the inversion results, and thick gray line indicates the optimal Vs profile.

The average RC values at JJU, as outlined in Table 10, consisted of three large positive values (0.30, 0.26, and 0.17) and one large negative RC ( $-0.17$ ). The initial large positive RC of 0.30 correlated with the transition from the surface outcrop to the rock mass or surface bedrock. At depths of 290–310 m, a substantial negative RC of  $-0.17$  suggests the presence of the LVL. This was followed by another large positive RC (0.26) at depths of 490–510 m. Ultimately, as the depth increased, there was a transition to the basement at approximately 690–710 m, indicated by an RC of 0.17. The final velocity model at JJU was interpreted as comprising five layers, inclusive of the deep basement, based on an analysis that encompassed both the models frequently represented in darker colors and the average RC values, as depicted in Figure 6. Similar to the other three sites previously discussed, a low-velocity layer was identified at the JJU site.

**Table 10.** Depth, shear velocity (Vs), and RC of JJU site.

Layer	Lower Limit Depth of Each Stratum (m)	Shear Velocity (m/s)	RC			
			B (1–2)	B (2–3)	B (3–4)	B (4–5)
1	160–180	700–900				
2	290–310	1300–1500	0/30			
<b>3</b>	<b>490–510</b>	<b>900–1100</b>		<b>(−) 0.17</b>		
4	690–710	1600–1800			0.26	
5	Basement	2300–2500				0.17

When comparing the JJB site with the JJU site, both situated in the northern region, notable differences in the LVL were observed. At the JJB site, the LVL begins at depths of 540–550 m, with a thickness of approximately 100 m and velocities ranging from 600 to 800 m/s. Conversely, at the JJU site, the LVL starts at depths of 490–510 m, spans around 200 m in thickness, and exhibits velocities of 900–1100 m/s. Although the starting depths of the LVL at both sites are relatively similar, there are discernible differences in both thickness and velocity.

#### 4.6. MRD

Figure 12 illustrates the observed and best-inverted HVSR curves for the small islands situated south of the Jeju region, as depicted in Figure 1. The observed HVSR curve featured a prominent peak at a frequency of 0.43 Hz, with corresponding peak amplitudes of 3.36, as indicated in Table 4.

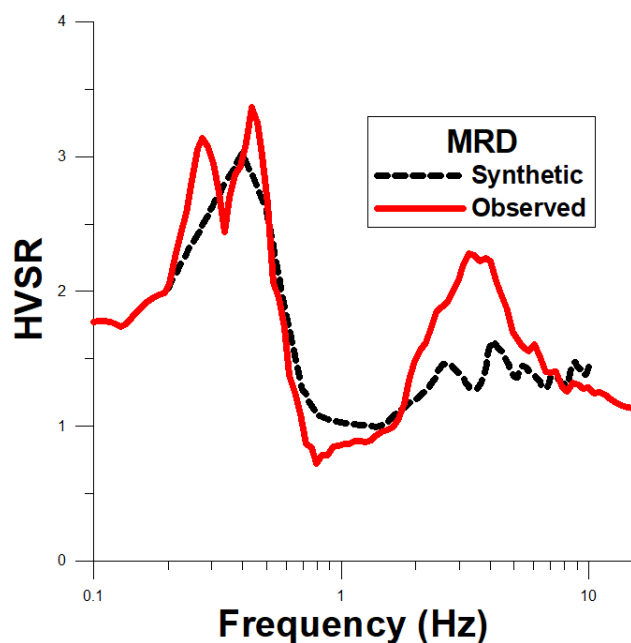


**Figure 12.** Observed and synthetic HVSRs of MRD site; the red line indicates the observed curve, and the black dotted line indicates the synthetic curve.

For the variance bounds from 0.25 to 2.5, the misfit sizes of the inversion using the MC simulations ranged from 80.41 to 2.22. The SA algorithm also produced misfit sizes for the best-fit inversion model within the same variance bounds. The misfit sizes, as well as the variations in amplitudes across the different frequency ranges, decreased with increasing the variance bounds for both algorithms.

Figure 13 displays the Vs profiles at the MRD site, portraying all the inverted and optimal Vs models. In determining the optimal shear velocity profile, the darker segments, which represent more frequently mapped areas, were given more weight. From the surface to depths of 60–80 m, the first layer exhibited velocities of 900–1100 m/s. Employing the site classification method based on the surface shear-wave velocity, as outlined in Table 5, the outcrops at the MRD sites (900–1100 m/s) were categorized as S<sub>B</sub>. The second layer, with velocities of 1200–1400 m/s, extended from 130–150 m depth. The third layer, the LVL, displaying velocities of 600–800 m/s and a significant velocity reduction of around 600 m/s, extended to depths of 290–310 m. This layer aligns with the typical LVL found throughout the Jeju region, as referenced in previous studies. With the further increase in depth, rapid velocity escalations were observed twice, at depths of 490–510 m and 690–710 m, with the latter marking the onset of the deep basement [45].

At the MRD site, as outlined in Table 11, there were four large positive RC values (0.13, 0.22, 0.21, and 0.17) and one large negative RC value (−0.30). The negative RC value denotes that the LVL, or the third layer, extended up to depths of 290–310 m with a velocity reduction of 600 m/s. This reduction was consistent with the −0.3 RC value, representing a very large absolute value. The deep basement initiated at depths of 690–710 m, with velocities ranging between 2200 and 2400 m/s.

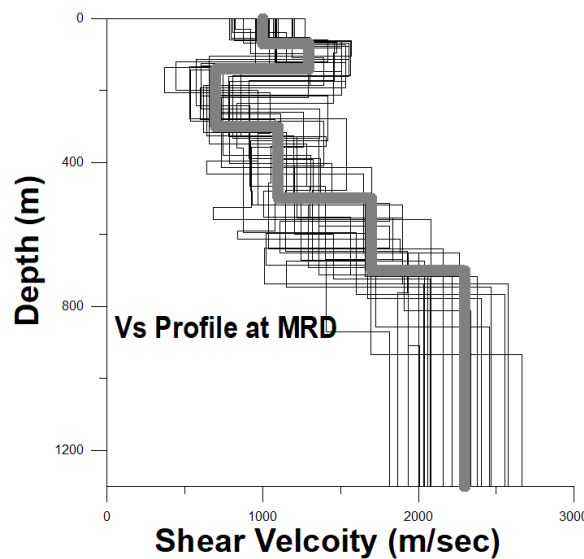


**Figure 13.** Estimated shear-wave velocity (Vs) profile from the inversion of MRD site; the thin lines indicate all the inversion results, and thick gray line indicates the optimal Vs profile.

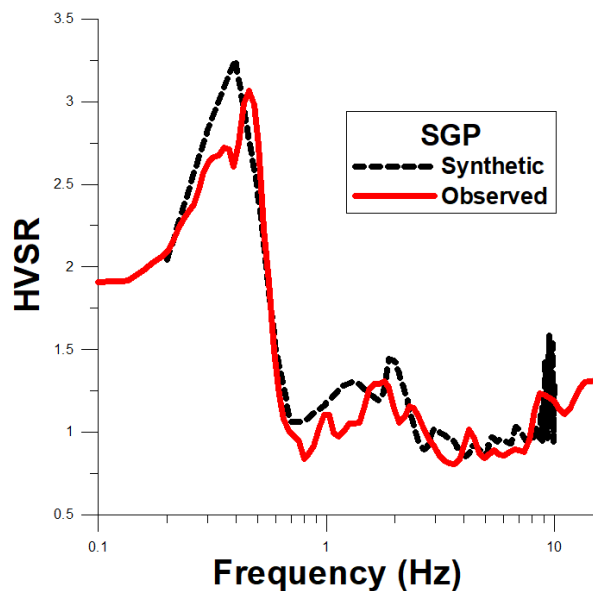
**Table 11.** Depth, shear velocity (Vs), and RC of MRD site.

Layer	Lower Limit Depth of Each Stratum (m)	Shear Velocity (m/s)	RC				
			B (1–2)	B (2–3)	B (3–4)	B (4–5)	B (5–6)
1	60–80	900–1100					
2	130–150	1200–1400	0.13				
3	390–410	600–800		(-) 0.30			
4	490–510	1000–1200			0.22		
5	690–710	1600–1800				0.21	
6	basement	2200–2400					0.17

The final velocity model at the MRD site was interpreted as comprising six layers, including the deep basement. This interpretation was based on an analysis that included both the models frequently represented in darker colors and the average RC values.

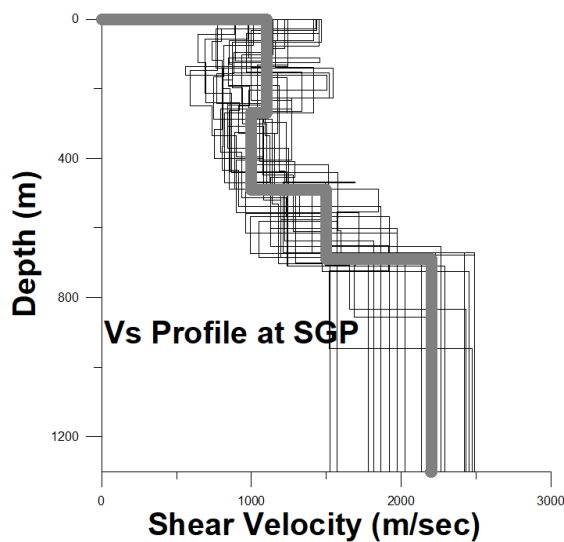
#### 4.7. SGP

Figure 14 presents both the observed and synthetic HVSR curves for the SGP site, located in the southern Jeju region, similar to the MRD site (Figure 1). The observed HVSR curve featured a distinct peak at a frequency of 0.42 Hz, with corresponding amplitudes of 3.88, as indicated in Table 4. To assess the misfit sizes of the inversion using the MC simulations, variance bounds ranging from 0.25 to 2.5 were applied, yielding values from 10.67 to 0.36. The SA algorithm also produced misfit sizes for the best-fit inversion model ranging from 2.36 to 0.21 within the same variance bounds. In line with findings from previous sites, an increase in the variance bounds correlated with a decrease in the misfit size for both algorithms. Despite the utilization of different inversion algorithms and the broad range of variances, both the observed and synthetic HVSR curves exhibited a strong correlation, particularly at higher frequencies, with minor deviations around 10 Hz and at resonance frequencies.



**Figure 14.** Observed and synthetic HVSRs of SGP site; the red line indicates the observed curve, and the black dotted line indicates the synthetic curve.

The Vs profile illustrated in Figure 15 presents the observed and optimal Vs models at the SGP site, with darker sections being given higher weights and indicating higher RC values. The subsurface analysis identified distinct stratigraphic layers. The first layer, extending from the surface to depths of 260–280 m, was characterized by velocities of 1000–1200 m/s. Utilizing the site classification method based on the outcrop shear-wave velocity, as indicated in Table 5, the outcrops at the SGP sites (1000–1200 m/s) were classified as S<sub>B</sub>. The second layer, which extended to depths of 480–500 m, featured a low-velocity layer (LVL) with velocities of 900–1100 m/s, slightly reduced compared to the first layer. The third layer, extending to depths of 680–700 m, marks the onset of the deep basement layer, with velocities ranging from 2100–2300 m/s [45].



**Figure 15.** Estimated shear-wave velocity (Vs) profile from the inversion of SGP site; the thin lines indicate all the inversion results, and thick gray line indicates the optimal Vs profile.

This study emphasized the examination of RC values and their correlation with other layer boundaries. The average RC values at the SGP site, as shown in Table 12, included two sizeable positive values (0.20 and 0.19) and a relatively small negative value (−0.05). Notably, the negative RC value of −0.05 at the SGP site was considerably smaller compared

to those at the other sites. Furthermore, the transition in velocity from the first layer to the LVL (second layer) at the SGP site was minimal, as indicated by the small RC value.

**Table 12.** Depth, shear velocity ( $V_s$ ), and RC of SGP site.

Layer	Lower Limit Depth of Each Stratum (m)	Shear Velocity (m/s)	RC		
			B (1–2)	B (2–3)	B (3–4)
1	260–280	1000–1200	(–) 0.07		
2	<b>480–500</b>	<b>900–1100</b>		0.20	
3	680–700	1400–1600			
4	Bedrock	2100–2300			0.19

The final velocity model for the SGP site was interpreted as comprising four distinct layers, including the deep basement layer. This interpretation was formulated by thoroughly analyzing both the frequently mapped modal models and the average RC values. Comparative analyses with other sites, such as the MRD in the southern region, provided valuable insights into regional variations in both the basement depth and LVL characteristics. Notably, the MRD and SGP sites exhibited almost identical basement depths.

#### 4.8. SSP Site

Figure 16 displays the observed and synthetic HVSR curves for the optimal  $V_s$  model at the SSP site, located in the eastern part of Jeju Island, as depicted in Figure 1. The observed HVSR curve showcased a notable peak at a frequency of 0.43 Hz, with a peak amplitude of 4.99, the highest among the nine sites examined in Table 4. For variance bounds ranging from 0.25 to 2.5, the misfit sizes of the inversion using the MC simulations varied from 338.41 to 1.38. Similarly, the SA algorithm yielded misfit sizes for the best-fit inversion model ranging from 205.04 to 1.24 within the same variance bounds. Although the peak amplitude near the resonance frequency closely matched between the observed and synthetic HVSR curves, the synthetic HVSR curve was slightly lower than the observed curve in the high-frequency range of 3–9 Hz.

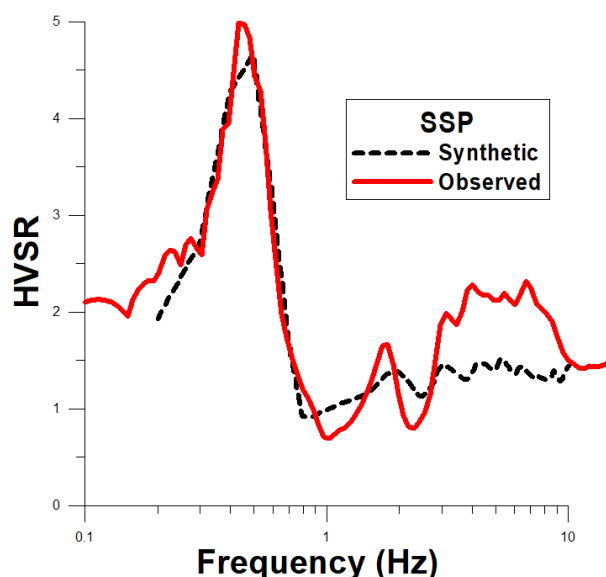


**Figure 16.** Observed and synthetic HVSRs of SSP site; the red line indicates the observed curve, and the black dotted line indicates the synthetic curve.

Figure 17 presents the  $V_s$  profile at the SSP site, illustrating all the inverted and optimal  $V_s$  models. In determining the optimal shear velocity profile, the darker regions, represent-

ing more frequently mapped areas, were given greater weight. The first layer, extending to depths of 40–60 m, formed a stratum with velocities of 900–1100 m/s. Employing the site classification method based on the outcrop shear-wave velocity, as indicated in Table 5, the outcrops at the SSP sites (900–1100 m/s) were categorized as  $S_B$ . The uncertainty associated with the first layer was notably larger than that of the subsequent deeper layers. The second layer extended to depths of 100–120 m, whereas the third layer, identified as the LVL with velocities of 600–800 m/s and a substantial velocity reduction of around 500 m/s, extended to depths of 320–340 m. With the further depth increase, the velocity doubled at depths of 460–480 m and 590–610 m, signaling the commencement of the deep basement [45].

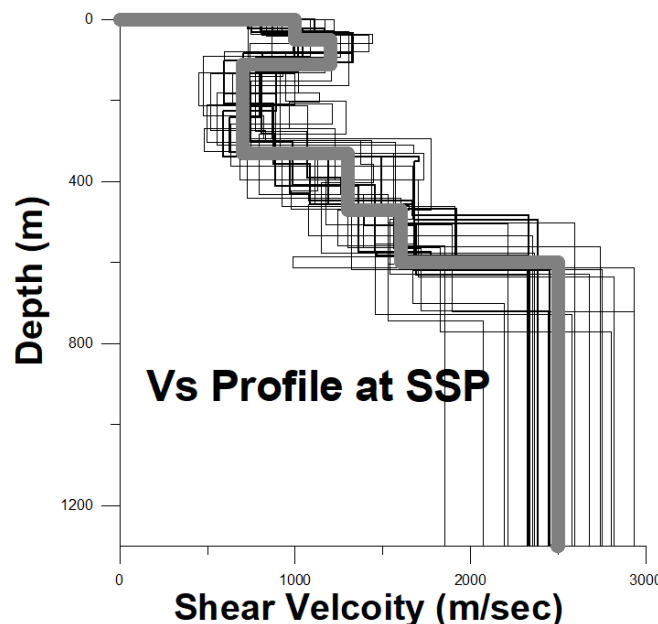


**Figure 17.** Estimated shear-wave velocity (Vs) profile from the inversion of SSP site; the thin lines indicate all the inversion results, and thick gray line indicates the optimal Vs profile.

The average RC values at the SSP site, as presented in Table 13, included four large positive values (0.10, 0.30, 0.10, and 0.22) and one large negative value (−0.26). The negative RC value of −0.26 indicates the presence of an LVL at this site, extending from 100–120 m to depths of 320–340 m. Additionally, with increasing the depth, the velocity rapidly doubled at depths of 460–480 m and 590–610 m, marking the onset of the deep basement.

**Table 13.** Depth, shear velocity (Vs), and RC of SSP site.

Layer	Lower Limit Depth of Each Stratum (m)	Shear Velocity (m/s)	RC				
			B (1–2)	B (2–3)	B (3–4)	B (4–5)	B (5–6)
1	40–60	900–1100					
2	100–120	1100–1300	0.10				
3	320–340	600–800		(−) 0.26		0.30	
4	460–480	1200–1400					0.10
5	590–610	1500–1700					
6	Basement	2400–2600					0.22

The final velocity model for the SSP site, as depicted in Figure 17, was interpreted as comprising six layers, inclusive of the deep basement. This interpretation was formulated by thoroughly analyzing both the frequently mapped models, represented by the darker-colored regions, and the average RC values.

Most previous studies have posited that both the U-formation, of marine origin, and the Seoguipo sedimentary layer contribute to characteristics of low velocity, low

gravity, and low resistivity, likely related to the LVL owing to their similar sedimentary origins [28,30–32]. However, other studies suggest that the area east of the Bukcheon-Pyoseon line does not contain a Seoguipo sedimentary layer [29,46,47]. Consequently, the LVL identified in this study at the SSP site was inferred to originate pre-dominantly from the U-formation with a marine origin, excluding the Seoguipo sedimentary layer.

As indicated in Table 4 and Figure 17, the SSP site exhibited the highest resonance frequency (0.43 Hz) and largest resonance amplitude (4.99 Hz) among the eight sites in the Jeju region, as well as the CJD site. Moreover, the LVL was located at the shallowest depth (320–340 m below the surface) and had the lowest Vs value (600–800 m/s). These characteristics, particularly the proximity of the LVL to the surface and its large resonance amplitude being significantly greater than unity, were likely directly related to the decision by the Korea Meteorological Administration (KMA) to close this site, aiming to minimize the distortion of the observed waveform.

Most prior studies suggest that the characteristics of the U-formation and Seoguipo sedimentary layer, including the low velocity, gravity, and resistivity, are associated with the LVL, whereas certain researchers dispute the presence of the Seoguipo sedimentary layer in the eastern region. This is further elaborated in the Discussion section.

#### 4.9. UDO Site

Figure 18 presents the observed and synthetic HVSR curves for the optimal Vs model at the UDO site, a small island located at the eastern end of the Jeju region, as illustrated in Figure 1. The observed HVSR curve featured a prominent peak at a frequency of 0.33 Hz (Table 4) with a peak amplitude of 3.20. For the variance bounds ranging from 0.25 to 2.5, the misfit sizes of the inversion using the MC simulations ranged from 349.54 to 2.29, whereas the SA algorithm yielded misfit sizes for the best-fit inversion model between 254.19 and 2.45 within the same variance bounds. Overall, the matching between the observed and synthetic curves was satisfactory, with minor discrepancies near the first peak of the double peak and in the frequency band above 1.5 Hz.

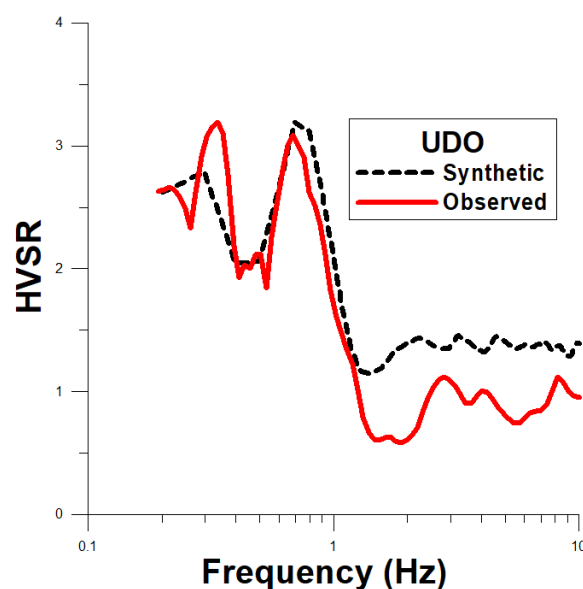


**Figure 18.** Observed and synthetic HVSRs of UDO site; the red line indicates the observed curve, and the black dotted line indicates the synthetic curve.

Figure 19 displays the Vs profile at the UDO site, showing all the inverted and optimal Vs models. The profile revealed a layer up to depths of approximately 140–160 m with velocities ranging from 400 to 600 m/s. By employing the site classification method on the outcrop shear-wave velocity, as indicated in Table 5, the outcrops at the UDO sites (1100–1300 m/s) were categorized as  $S_C$ , ranking it as the softest site class among the nine

sites investigated. The second layer, extending to depths of 240–260 m, exhibited velocities of 900–1100 m/s. The third layer, characterized by velocities of 1200–1400 m/s, extended to depths of 390–410 m. The fourth layer, with velocities of 1500–1700 m/s, extended to depths of 590–610 m. Subsequently, the fifth layer, identified as the LVL with velocities of 900–1100 m/s, extended to depths of 790–810 m. This LVL displayed a significant velocity contrast of around 600 m/s on average compared to the overlying layer. Finally, the velocity increased remarkably, connecting to the basement at depths of 2100–2300 m/s [45].

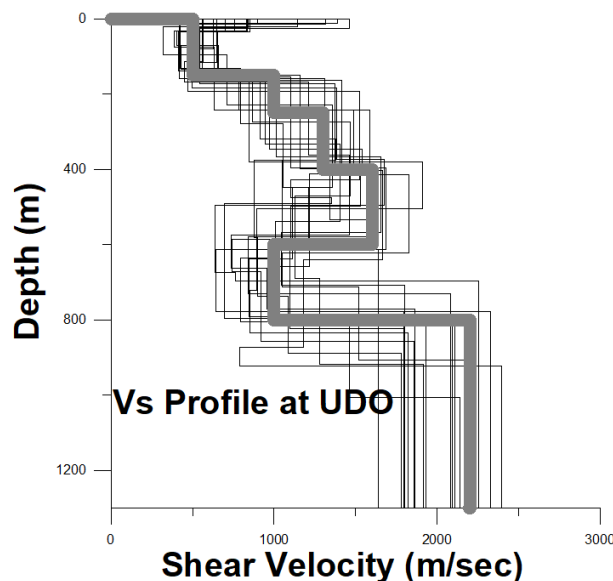


**Figure 19.** Estimated shear-wave velocity (Vs) profile from the inversion of UDO site; the thin lines indicate all the inversion results, and thick gray line indicates the optimal Vs profile.

The RC values for the UDO site, as listed in Table 14, encompassed four prominent positive peaks (0.33, 0.13, 0.10, and 0.38) and one substantial negative peak (−0.23). The negative RC value of −0.23 signals the presence of an LVL, extending from depths of 590–610 m to 790–810 m, approaching the basement.

**Table 14.** Depth, shear velocity (Vs), and RC of UDO sites.

Layer	Lower Limit Depth of Each Stratum (m)	Shear Velocity (m/s)	RC				
			B (1–2)	B (2–3)	B (3–4)	B (4–5)	B (5–6)
1	140–160	400–600	0.33				
2	240–260	900–1100		0.13			
3	390–410	1200–1400			0.10		
4	590–610	1500–1700				(−) 0.23	
5	<b>790–810</b>	<b>900–1100</b>					<b>0.38</b>
6	Bedrock	2100–2300					

The UDO site was distinguished by its unique stratigraphic characteristics, which deviated from prior expectations of the absence of the Seoguipo sedimentary layer. These findings suggest the possibility of an LVL at the UDO site, potentially formed by recent local magmatic intrusion events rather than being solely attributed to the U-formation of marine origin. This hypothesis and its implications are further explored in the Discussion section.

## 5. Discussion

This study aimed to confirm the presence of an LVL across various sites in the Jeju area. The inversion analysis results substantiated the existence of an LVL at all eight sites examined, aligning with findings from previous research, with the exception of the CJD

site. The analysis of the multilayer structure revealed that the velocity of the LVL varied substantially, ranging from 600 to 1100 m/s, and was distributed across depths of from 320 to 810 m from the surface, as detailed in Tables 7–14. The identification of the LVL at the sites in the eastern, western, southern, and northern regions of Jeju confirms its widespread presence throughout the area. Note that of the eight sites considered in this research, two are islands, and six are located closer to the coast than those examined in previous studies.

Regarding the SSP site, most prior studies have suggested that both the U-formation, originating from marine deposits, and the Seoguipo sedimentary layer exhibit low velocity, gravity, and resistivity. These characteristics are likely related to the LVL due to their shared sedimentary origin [28,30,32,46]. However, some researchers have posited that the area east of the Bukcheon–Pyoseon line lacks a Seoguipo sedimentary layer [31,47]. As indicated in Table 4 and Figure 17, the SSP site exhibited the highest resonance frequency (0.43 Hz) and largest resonance amplitude (4.99) among all the eight sites in the Jeju region, including the CJD site. Additionally, the LVL at the SSP site was located at a relatively shallow depth (320–340 m below the surface) and had the lowest Vs values (600–800 m/s). These characteristics, especially the proximity of the LVL to the surface and its notably large resonance amplitude, are likely directly related to the decision by the KMA to close this site to minimize waveform distortion in seismic monitoring.

The UDO site, situated east of the Bukcheon–Pyoseon line like the SSP site, falls within a region where previous studies did not anticipate the presence of a Seoguipo sedimentary layer. Consequently, the low-velocity layer (LVL) identified at the UDO site is likely a formation of marine origin, akin to the U-formation.

However, when compared to other sites, the UDO site exhibits unique stratigraphic features, as detailed below (refer to Table 14 and Figure 19):

1. The UDO site has the deepest basement among the eight sites examined, with the lowest basement velocity, ranging from 2100 to 2300 m/s.
2. The LVL at the UDO site shows a significant velocity reduction of approximately 600 m/s compared to the layer above it and possesses a relatively high thickness of around 200 m.
3. Notably, the LVL is situated directly above the basement, whereas the layer immediately above the basement across the Jeju region is typically a tuff layer that is present throughout the Jeju region.

Given these distinct stratigraphic features, several geological hypotheses could explain the presence of the LVL at the UDO site, differing from the expected U-formation. The first hypothesis considers the possibility of seawater fluid injection or groundwater storage due to the proximity of the site to the coast, although this is unlikely due to the considerable depth of the LVL. A second possibility involves the development of a local fault or fracture zone, yet this is deemed improbable due to the lack of significant orogeny in the area. The third and most plausible hypothesis attributes the LVL to local intrusive magma that is yet to fully consolidate. Considering the frequent occurrence of intrusive magma injections in the Jeju region over extended geological periods, it is highly likely that the LVL at the UDO site was formed by a recent local magmatic intrusion rather than by a U-formation of marine origin. Future research may provide further insights into this topic, potentially yielding a clearer understanding of the unique characteristics of the UDO site.

The findings from the eight Jeju sites, particularly the SSP and UDO sites, demonstrate that a substantial thickness of the LVL is a consistent feature across all sites, highlighting a complex multilayer structure. Consequently, the existence of such layers may present challenges to various geophysical interpretation methods. These include borehole analysis [32], gravity and magnetic surveys [27], gravity studies [28], paleomagnetic research [29], seismic investigations [30], magnetotelluric (MT) assessments [31], and deep resistivity soundings [32]. Specifically, these challenges become evident when these methods are applied with oversimplifications, such as assuming a two-layer structure.

The basement depth in the Jeju area varies, ranging from 590 to 810 m below the surface, with basement velocities of 2100–2700 m/s, as detailed in Tables 7–14. This variability is

especially pronounced when excluding the UDO site, which has a depth of 790–810 m. Excluding the UDO site, the basement depth of the remaining seven sites lies within a relatively narrow range of 590–710 m. This uniformity in the basement depth was observed across all Jeju sites, with the exception of the UDO site. Notably, only the CJD site, which possesses a geologically distinct tectonic structure, was included for comparative purposes. The Vs profiles indicate significant differences between the eight Jeju sites in terms of the shear velocity and the presence or absence of an LVL structure, thereby enhancing the reliability of this study.

The resolution of the highly ill-posed inversion process in this study was achieved through the implementation of four key strategies. These strategies included the application of two distinct inversion algorithms, the allowance of broad variance ranges in the observed HVSR data, the determination of an optimal initial parameter value range based on previous studies, and the inclusion of a preliminary random search phase. These innovative strategies effectively addressed the challenges inherent in the highly ill-posed inversion process, leading to satisfactory results.

In addition, this study explored the interpretation of various Vs models by employing two specific approaches. These approaches comprised a weighting scheme for the more frequently mapped darker profiles as well as the use of the RC index. Combining these tactics facilitated the attainment of an optimal Vs model with a high degree of consistency.

## 6. Conclusions

1. An LVL was conclusively identified at all the eight sites surveyed across the eastern, western, southern, and northern regions of the Jeju area. However, the origin of the LVL at the UDO site appears to differ from the other sites. The velocity of the LVL across these sites spans from 700 to 1100 m/s, with an average thickness of approximately 160–300 m. This finding highlights the widespread presence of the LVL throughout the Jeju region, albeit with variations in its geological origin, particularly at the UDO site.
2. As discussed in this study, the unique stratigraphy of the UDO site contrasts with prior assumptions regarding the Seoguipo sedimentary layer. This contrast suggests the existence of a low-velocity layer potentially formed by recent local magmatic intrusion events rather than the anticipated marine-origin U-formation.

This hypothesis represents a significant departure from earlier understandings and warrants further exploration in the discussion section. The implication that the LVL at the UDO site might be a result of geologically recent processes, rather than sedimentary deposits, opens up new avenues for understanding the geophysical characteristics of the region.

3. The basement depth in the Jeju region varies from 590 m to 810 m below the surface, with a broad range of values observed. Excluding the UDO site, the basement depths of the other seven sites fall within a more confined range of 590–710 m, demonstrating a relatively narrow range of basement depths. The CJD site, characterized by a geologically distinct tectonic structure, was included primarily for comparison. The Vs profile at the CJD site distinctly differed from the eight Jeju sites in terms of the shear velocity and the absence of an LVL structure, thereby enhancing the reliability of this research.
4. The resolution of the highly ill-posed inversion process was successfully achieved through the implementation of four key strategies. These included the application of two different inversion algorithms, the allowance of broad variance ranges in the observed HVSR curves, the determination of optimal initial parameter value ranges based on prior studies, and the execution of a preliminary random search. Furthermore, this study employed a weighting scheme for more frequently mapped darker profiles and utilized the RC index for interpreting various Vs models. This approach enabled us to achieve an optimal Vs model characterized by a high consistency.

5. This research has yielded valuable geological insights, extending beyond the shallow layers to the basement at depths greater than 700 m. Such comprehensive data significantly contribute to microzonation analysis in the Jeju region, including site amplification and site attenuation (kappa value), thereby aiding in the development of seismic design codes or standards. The findings from this study are instrumental in enhancing our understanding of the overall seismic hazards in the Jeju region.
6. In this study, the number of layers at the nine sites was interpreted to range between four and six layers, thus validating the initial assumption of seven layers as a reasonable starting point. However, the geological aspect of stratigraphic diversity should be considered, and the number of parameters or layers should be minimized for the efficiency of the inversion process. Therefore, determining the appropriate maximum number of layers before inversion through numerous initial trial-and-error inversion processes is of significant importance.

**Author Contributions:** Conceptualization, J.K. and G.N.; methodology, J.K.; software, J.K.; validation, G.N. and H.J.; formal analysis, J.K.; investigation, G.N.; resources, H.J.; data curation, D.P.; writing—original draft preparation, J.K.; writing—review and editing, D.P. and H.J.; visualization, D.P.; supervision, G.N.; project administration, H.J.; funding acquisition, D.P. All authors have read and agreed to the published version of the manuscript.

**Funding:** This work was supported by the Korea institute of Energy Technology Evaluation and Planning (KETEP) and the Ministry of Trade, Industry & Energy (MOTIE) of the Republic of Korea (No.2021171020001A). Also, this work was supported by the National Research Foundation of Korea (NRF) grant funded by the Korean government (MSIT) (NRF-2021R1G1A1014385).

**Data Availability Statement:** Data are contained within the article.

**Conflicts of Interest:** Author Gitae Nam was employed by the company Seoul Metropolitan Council, Urban Safety & Construction Committee. The remaining authors declare that the research was conducted in the absence of any commercial or financial relationships that could be construed as a potential conflict of interest.

## References

1. Marco, Z.; Giuseppe, C.P.; Giuseppe, T.; Marco, S. On the influence of shallow underground structures in the evaluation of the seismic signals. *Ing. Sismica* **2021**, *38*, 23–35.
2. Lermo, J.; Francisco, J.C. Site effect evaluation using spectral ratios with only one station. *Bull. Seismol. Soc. Am.* **1993**, *83*, 1574–1594. [[CrossRef](#)]
3. Bonilla, L.F.; Steidl, J.H.; Lindley, G.T.; Tumarkin, A.G.; Archuleta, R.J. Site amplification in the San Fernando Valley, California: Variability of site effect estimation using the S-wave, coda, and H/V methods. *Bull. Seismol. Soc. Am.* **1997**, *87*, 710–730. [[CrossRef](#)]
4. Hartzell, S.; Cranswick, E.; Frankel, D.; Meremonte, M. Variability of site response in the Los Angeles Urban area. *Bull. Seismol. Soc. Am.* **1997**, *87*, 1377–1400. [[CrossRef](#)]
5. Seed, H.B.; Toro, M.P.; Sun, J.L. Relationship between soil conditions and earthquake motions in Mexico City in the earthquake of Sept. 19, 1985. *Earthq. Spectra* **1988**, *4*, 687–729. [[CrossRef](#)]
6. Tucker, B.D.; King, J.L. Dependence of sediment filled valley response on input amplitude and valley properties. *Bull. Seismol. Soc. Am.* **1984**, *74*, 153–165. [[CrossRef](#)]
7. Phillips, S.C.; Aki, K. Sites amplification of coda waves from local earthquakes in central California. *Bull. Seismol. Soc. Am.* **1986**, *76*, 627–648. [[CrossRef](#)]
8. Su, F.; Anderson, J.G.; Brune, J.N.; Zeng, Y. A comparison of direct S-wave and coda wave site amplification determined from aftershocks of the Little Skull Mountain earthquake. *Bull. Seismol. Soc. Am.* **1996**, *86*, 1006–1018. [[CrossRef](#)]
9. Hennino, R.; Tregoures, N.; Shapiro, N.; Margerin, L.; Campillo, M.; van Tiggelen, B.; Weaver, R. Observation of equipartition of seismic waves. *Phys. Rev. Lett.* **2001**, *86*, 3447–3450. [[CrossRef](#)]
10. Margerin, L.; Campillo, M.; van Tiggelen, B.V.; Hennino, R. Energy partition of seismic coda waves in layered media: Theory and application to Pinyon Flats Observatory. *Geophys. J. Int.* **2009**, *177*, 571–585. [[CrossRef](#)]
11. Poggi, V.; Edwards, B.; Fäh, D. Derivation of a reference shear wave velocity model from empirical site amplification. *Bull. Seismol. Soc. Am.* **2011**, *101*, 258–274. [[CrossRef](#)]
12. Matsushima, S.; Hirokawa, T.; Martin, F.D.; Sánchez-Sesma, F.J. The effect of lateral heterogeneity on horizontal-to-vertical spectral ratio of microtremors inferred from observation and synthetics. *Bull. Seismol. Soc. Am.* **2014**, *104*, 381–393. [[CrossRef](#)]

13. Cavallaro, A.; Grasso, S.; Sammito, M.S.V. A Seismic Microzonation Study for Some Areas Around the Mt. Etna Volcano on the East Coast of Sicily, Italy. In Proceedings of the 4th International Conference on Performance Based Design in Earthquake Geotechnical Engineering, Beijing, China, 15–17 July 2022. [CrossRef]
14. Yamanaka, H.; Takemura, M.; Ishida, H.; Niwa, M. Characteristics of long-period microtremors and their applicability in exploration of deep sedimentary layers. *Bull. Seismol. Soc. Am.* **1994**, *84*, 1831–1841. [CrossRef]
15. Dolenc, D.; Dreger, D. Microseisms observations in the Santa Clara Valley, California. *Bull. Seismol. Soc. Am.* **2005**, *95*, 1137–1149. [CrossRef]
16. Ibs-Von Seht; Wohlenberg, J. Microtremor measurements used to map thickness of soft sediments. *Bull. Seismol. Soc. Am.* **1999**, *89*, 250–259. [CrossRef]
17. Scherbaum, F.; Hinzen, K.G.; Ohrnberger, M. Determination of shallow shear wave velocity profiles in the Cologne, Germany area using ambient vibrations. *Geophys. J. Int.* **2003**, *152*, 597–612. [CrossRef]
18. Fäh, D.; Kind, F.; Giardini, D. A theoretical investigation of average H/V ratios. *Geophys. J. Int.* **2001**, *145*, 535–549. [CrossRef]
19. Arai, H.; Tokimatsu, K. S-wave velocity profiling by inversion of microtremor H/V spectrum. *Bull. Seismol. Soc. Am.* **2004**, *94*, 53–63. [CrossRef]
20. Sanchez-Sesma, F.J.; Perez-Ruiz, J.A.; Luzon, F.; Campillo, M.; Rodriguez-Castellanos, A. Diffuse fields in dynamic elasticity. *Wave Motion* **2008**, *45*, 641–654. [CrossRef]
21. Sanchez-Sesma, F.J.; Rodriguez, M.; Iturraran-Viveros, U.; Luzon, F.; Campillo, M.; Margerin, L.; Garcia-Jerez, A.; Suarez, M.; Santoyo, M.A.; Rodriguez-Castellanos, A. A theory for microtremor H/V spectral ratio: Application for a layered medium. *Geophys. J. Int.* **2011**, *186*, 221–225. [CrossRef]
22. Kawase, H.; Matsushima, S.; Satoh, T.; Sánchez-Sesma, F.J. Applicability of theoretical horizontal-to-vertical ratio of microtremors based on the diffuse field concept to previously observed data. *Bull. Seismol. Soc. Am.* **2011**, *101*, 3092–3103. [CrossRef]
23. Kawase, K.; Sánchez-Sesma, F.J.; Matsushima, S. The optimal use of horizontal-to-vertical spectral ratios of earthquake motions for velocity inversions based on diffuse-field theory for plane waves. *Bull. Seismol. Soc. Am.* **2011**, *101*, 2001–2014. [CrossRef]
24. Lontsi, A.M.; Sanchez-Sesma, F.J.; Molina-Villegas, J.C.; Ohrnberger, M.; Kruger, F. Full microtremor H/V(z,f) inversion for shallow subsurface Characterization. *Geophys. J. Int.* **2015**, *202*, 298–312. [CrossRef]
25. KIGAM. 1:250,000 Explanatory Note of the Jeju; KR-00(B)-01; Korea Institute of Geology, Mining and Materials: Daejeon, Republic of Korea, 2000; p. 59.
26. Oh, J.; Yi, S.; Yoon, S.; Koh, G.-W.; Yun, H.; Lee, J.-D. Subsurface stratigraphy of Jeju Island. *J. Geol. Soc. Korea* **2000**, *36*, 181–194. (In Korean)
27. Kwon, B.-D.; Lee, H.-S. Investigation of subsurface structure of Cheju Island by gravity and magnetic methods. *J. Korean Earth Sci. Soc.* **1997**, *18*, 217–237. (In Korean)
28. Lee, K.; Jeong, B.I.; Choi, K.S.; Lee, S.K. A study of gravity and geomagnetism of Jeju Island. *J. Geol. Soc. Korea* **1983**, *19*, 1–10.
29. Kim, I.S.; Lee, D. Magnetostratigraphy and AMS of the Seoguipo Formation and Seoguipo Trachyte of Jeju Island. *J. Geol. Soc. Korea* **2000**, *36*, 163–180. (In Korean)
30. Kim, K.Y.; Hong, M.H. Shear-wave velocity of Jeju Island. *Geosciences J.* **2012**, *16*, 35–45. [CrossRef]
31. Choi, J.; Kim, H.J.; Nam, M.J.; Lee, T.J.; Ham, N.; Lee, S.K.; Song, Y.; Suh, J.H. A study on geoelectrical structure of Jeju Island using 3D MT inversion of 2D profile data. *Malli-Tamsa* **2007**, *10*, 268–274. (In Korean)
32. Lee, K.; Kim, H.S. Deep electrical soundings in the Cheju Island. *J. Geol. Soc. Korea* **1993**, *29*, 30–38.
33. Konno, K.; Ohmachi, T. Ground-motion characteristics estimated from spectral ratio between horizontal and vertical components of microtremor. *Bull. Seismol. Soc. Am.* **1998**, *88*, 228–241. [CrossRef]
34. Wathelet, M.; Chatelain, J.L.; Cornou, C.; Giulio, G.D.; Guillier, B.; Ohrnberger, M.; Savvaïdis, A. Geopsy: A user-friendly open-source tool set for ambient vibration processing. *Seismol. Res. Lett.* **2020**, *91*, 1878–1889. [CrossRef]
35. Menke, W. *Geophysical Data Analysis: Discrete Inverse Theory*; Academic Press: San Diego, CA, USA, 1989.
36. Tarantola, A. *Inverse Problem Theory and Methods for Model Parameter Estimation*; Society of Industrial and Applied Mathematics: Philadelphia, PA, USA, 2005; p. 342.
37. Kirkpatrick, S.C.; Gelatt, D.; Vecchi, M.P. Optimization by simulated annealing. *Science* **1983**, *220*, 671–680. [CrossRef]
38. Mosegaard, K.; Sambridge, M. Monte Carlo analysis of inverse problems. *Inverse Probl.* **2002**, *18*, 29–54. [CrossRef]
39. Nils, R.; Park, C.B. Fast simulated anneal inversion of surface waves on pavement using phase-velocity spectra. *Geophysics* **2006**, *71*, 49–58.
40. Pei, D. Modeling and Inversion of Dispersion Curves of Surface Waves in Shallow Site Investigations. Ph.D. Thesis, University of Nevada, Reno, NV, USA, 2007; p. 165.
41. Pei, D.; Louie, J.N.; Pullammanappallil, S.K. 1-D inversion of shallow surface wave dispersion curves using a simulated annealing optimization method. In *SEG Technical Program Expanded Abstracts 2005*; Society of Exploration Geophysicists: Houston, TX, USA, 2005; pp. 1172–1175.
42. Arai, H.; Tokimatsu, K. S-wave velocity profiling by joint inversion of microtremor dispersion curve and horizontal-to-vertical (H/V) spectrum. *Bull. Seismol. Soc. Am.* **2005**, *95*, 1766–1778. [CrossRef]
43. Parolai, S.; Richwalski, S.M.; Milkereit, C.; Fäh, D. S-wave velocity profile for earthquake engineering purposes for the Cologne area (Germany). *Bull. Earthq. Eng.* **2006**, *4*, 65–94. [CrossRef]
44. MOLIT. *Korean Building Code, Building Structural Code Revision*; MOLIT: Seoul, Republic of Korea, 2016.

45. Sivaram, K.; Mahesh, I.P.; Rai, S.S. Stability assessment and quantitative evaluation of H/V spectral ratios for site response studies in Kumaon Himalaya, India using ambient noise recorded by a broadband seismograph network. *Pure Appl. Geophys.* **2012**, *169*, 1801–1820. [[CrossRef](#)]
46. Gang, S.R.; Jung, G.G.; Yoon, S. Benthic foraminiferal fauna from drilled cores of Jeju Island, Korea. *J. Paleontol. Soc. Korea* **2002**, *18*, 1–10. (In Korean)
47. Yi, S.; Yun, H.; Yoon, S. Calcareous nanoplankton from Seoguipo Formation of Cheju Island, Korea and its paleo oceanographic implementations. *Paleontol. Res.* **1998**, *2*, 253–265.

**Disclaimer/Publisher's Note:** The statements, opinions and data contained in all publications are solely those of the individual author(s) and contributor(s) and not of MDPI and/or the editor(s). MDPI and/or the editor(s) disclaim responsibility for any injury to people or property resulting from any ideas, methods, instructions or products referred to in the content.